IEEE Access
Multidisciplinary | Rapid Review | Open Access Journal

Received November 23, 2019, accepted December 31, 2019, date of publication January 7, 2020, date of current version January 28, 2020.

Digital Object Identifier 10.1109/ACCESS.2020.2964641

Development of a Novel End-Effector for an On-Orbit Robotic Refueling Mission

JINGUO LIU[1,2], (Senior Member, IEEE), YUCHUANG TONG[1,2,3], YUNJUN LIU[1,2,3], AND YUWANG LIU[1,2], (Member, IEEE)

[1]State Key Laboratory of Robotics, Shenyang Institute of Automation, Chinese Academy of Sciences, Shenyang 110016, China
[2]Institutes for Robotics and Intelligent Manufacturing, Chinese Academy of Sciences, Shenyang 110169, China
[3]University of the Chinese Academy of Sciences, Beijing 100049, China

Corresponding author: Jinguo Liu (liujinguo@sia.cn)

This work was supported in part by the National Key Research and Development Program of China under Grant 2018YFB1304600, in part by the Natural Science Foundation of China under Grant 51775541, and in part by the Chinese Academy of Sciences (CAS) Interdisciplinary Innovation Team under Grant JCTD-2018-11.

ABSTRACT At present, the space station on-orbit service is still rapidly developing, and on-orbit refueling operation has not been fully realized. During the process of an on-orbit robotic refueling mission, the pipe disconnectors are artificially docked, and the problems of low efficiency and a long operation period are common. From the perspective of bionics, this paper studies the kinematics of the upper limbs in the manual docking process of the pipeline quick disconnector and analyses the redundant degrees of freedom in the manual docking process. In this paper, without changing the original structure of the quick disconnector, a five-degrees-of-freedom multifunctional end-effector imitating the human hand with a compact structure and a light weight was created, which can realize the automatic docking of the quick disconnector in the pipeline. The quick disconnector docking in the refueling system is simplified from the original manual, two-handed operation to a single-end-effector operation with a single mechanical arm. Compared with a dual-arm robot, a single-arm robot has the advantages of internal force sealing, a stable structure, a higher docking accuracy and a lower cost. The common rigid body contact collision dynamics problem is thus studied. The contact dynamics model between the ''quick disconnector and the robot end-effector'' is established by the equivalent spring damping model method. The experimental prototype was developed according to the structure of the end-effector to complete the construction of the refueling robot experimental platform. A simulation and experiment were conducted to verify the advantages and effectiveness of the structure.

INDEX TERMS On-orbit servicing, robotic refueling mission, end-effector, imitating human hand, collision dynamics analysis.

I. INTRODUCTION

Statistics have shown that in the past decade, an average of 100 satellites (from 78 to 130) have been launched each year, most of which did not encounter any major problems. However, a few satellites experienced operational anomalies or even varying degrees of failure [1]. In the past, transmitter failure was the most common cause of mission failure. However, in recent years the rate of on-orbit failures has exceeded the rate of launch failures for the first time [2], causing billions of dollars in losses [3]. Due to the lack of so-called on-orbit service (OOS) opportunities, parts of the malfunctioning spacecraft continue to work in a weakened state or can barely complete any work [4], [5]. It is worth noting that this complex space mission has promoted the development of new space robotics technology and several experimental demonstration missions, including manned and unmanned missions [6], [7]. To support current and future spacecraft development, the concept of on-orbit service (OOS) infrastructure has been proposed to alleviate the current deficiencies and shortcomings that currently exist in the aerospace industry [8]. An OOS is a space mission for space robots that can extend the life of orbiting satellites through robotic refueling missions, repair, inspection, orbital maintenance or satellite reuse and may reduce the rate of space debris generation [9].

Currently, the scale of engineering development for spacecraft in the field of on-orbital services is very large, and the research achievements at the domestic and international levels are remarkable. Regarding the concept of

The associate editor coordinating the review of this manuscript and approving it for publication was Rosario Pecora.

on-orbit service, researchers have done significant research from different angles. Li *et al.* [10] attempted to summarize all currently reported engineering development projects on OOS. Graham and Kingston [11] analysed the research background of these maintenance tasks and life extension tasks. Zhang and Liu [12] proposed a new perspective, in which berths should be considered in the motion planning strategy of capturing targets. Da *et al.* [13] analysed the dynamic influence of the robot manipulator's motion attitude. Yao *et al.* [14] studied the OOS system evaluation and optimization method based on a life cycle simulation under uncertainty. To ensure the safe docking of non-cooperative target satellites, Benninghoff *et al.* [15] designed and developed a system for measuring the guidance, navigation and control using optical sensors. Li *et al.* [16]–[18] proposed a new configuration with a large-mass-ratio moving mass and reactive jet for the control problem of aircraft. Xu *et al.* [19] developed an improved modal method for on-orbit maintenance tasks to solve the inverse kinematics method of a hyper-redundant space manipulator. Saleh *et al.* [20] proposed a new customer-centric on-orbit service perspective. Since the failure of geostationary orbit (GEO) spacecraft will result in huge economic losses and other adverse effects, Xu *et al.* [21] proposed a space robot service system and developed key attitude measurements and control algorithms. Ellery *et al.* [22] specifically considered the recent high incidence of on-orbit failures of geostationary communication platforms and determined that only OOS can mitigate current and future failures. OOS was evaluated by Andrew *et al.* [23] in the current satellite paradigm, and a new paradigm was proposed. Hirzinger *et al.* [24] outlined long-term space robot projects and the latest achievements of the DLR robotics laboratory. Stoll *et al.* [25] verified the applicability of OOS in a remote presentation, that is, space-based unattended remote operations in real time.

Robotic services on non-cooperative satellites remain an open research area facing many technical challenges. One of the most significant challenges is to ensure that the maintenance spacecraft can safely and reliably dock with the target spacecraft or capture the target to stabilize it for subsequent maintenance [26]. Every launched satellite will face the problem of fuel exhaustion, in which case the satellite has to be decommissioned, even if it is still functioning properly. Many studies [27]–[29] have indicated the potential value of repairing damaged spacecraft in flight from the perspective of cost-effectiveness. Saleh *et al.* [30], [31] proposed a model including a risk and uncertainty analysis. For these reasons, the National Aeronautics and Space Administration (NASA) recognized the importance of protecting the space resources of robots in orbital maintenance operations as early as the 1980s [32], [33]. Among them, on-orbit robotic refueling mission can extend the service life of the satellite, resulting in a considerable economic saving effect [34]. NASA used the ISS's Canadarm2 and Dextre robots to perform an experimental demonstration of a robotic refueling mission [35]. The European Space Agency (ESA) believes that on-orbital robotic refueling missions have promising capabilities for low-earth orbit through spacecraft services. ESA aims to conceive and promote standard refueling regulations on satellite platforms and scientific spacecraft that can be installed on current and future European commercial GEO satellites. This refueling approach is in line with the European industry (OHB, Thales Alenia Space) and is expected to merge with European commercial operators as the first step towards becoming an international standard [36]. Specifically, the definition of an on-orbit robotic refueling mission can be extended to the scope of manned space flight, providing fuel and other essentials for spacecraft [10]. On-orbit refueling includes the following parts: the capture mechanism, a standard docking interface for mechanical connections, a standard interface for fuel connections, a propellant refueling and transfer process, and replenishment of other consumables.

Propellant in orbit replenishment technology is a very difficult technology with very high reliability requirements. The realization of on-orbit replenishment technology will greatly increase the manoeuvrability of spacecraft, improve the efficiency of satellites, and improve the economic benefits of spacecraft. It is thus an indispensable technology for permanent space stations. This section will specifically introduce the scheme design and principle analysis of the on-orbit robotic refueling mission (which is the application of an end-effector imitating the human hand), thus laying the foundation for the system. The application prospect of on-orbit replenishment technology in the aerospace field is very promising. The main application directions of this technology are as follows: (1) On-orbit replenishment of satellites with multiple orbital manoeuvres. (2) On-orbit replenishment of long-lived satellites. (3) Space refueling for deep space detectors.

The filling process of the on-orbit robotic refueling mission scheme designed in this paper is as follows and is shown in Figure 1.

(1) First, the target aircraft is captured by the electrostatic adsorption device. Under the guidance of binocular stereo vision, the target aircraft is captured by a robotic arm with an electrostatic adsorption device, so that the on-orbit aircraft and the target aircraft remain relatively stationary.

(2) The robotic arm carries a refueling tool (clamp) to the target aircraft to be refuelled, and the corresponding pose information is obtained by a binocular vision measurement of the ''refueling disconnector''. Then, trajectory planning of the robot arm is performed to calculate a reasonable trajectory for the arm effector refueling, after which the mechanical arm follows the path to take the refueler holder and sends it to the designated position.

(3) The position of the refueling disconnector is obtained by the camera on the replaceable end tool, and then the refueling disconnector on the refueling effector is used for refueling.

(4) After target separation and target refueling, the refueling effector loosens the disconnector and closes the valve. The electrostatic adsorption device is powered off to release

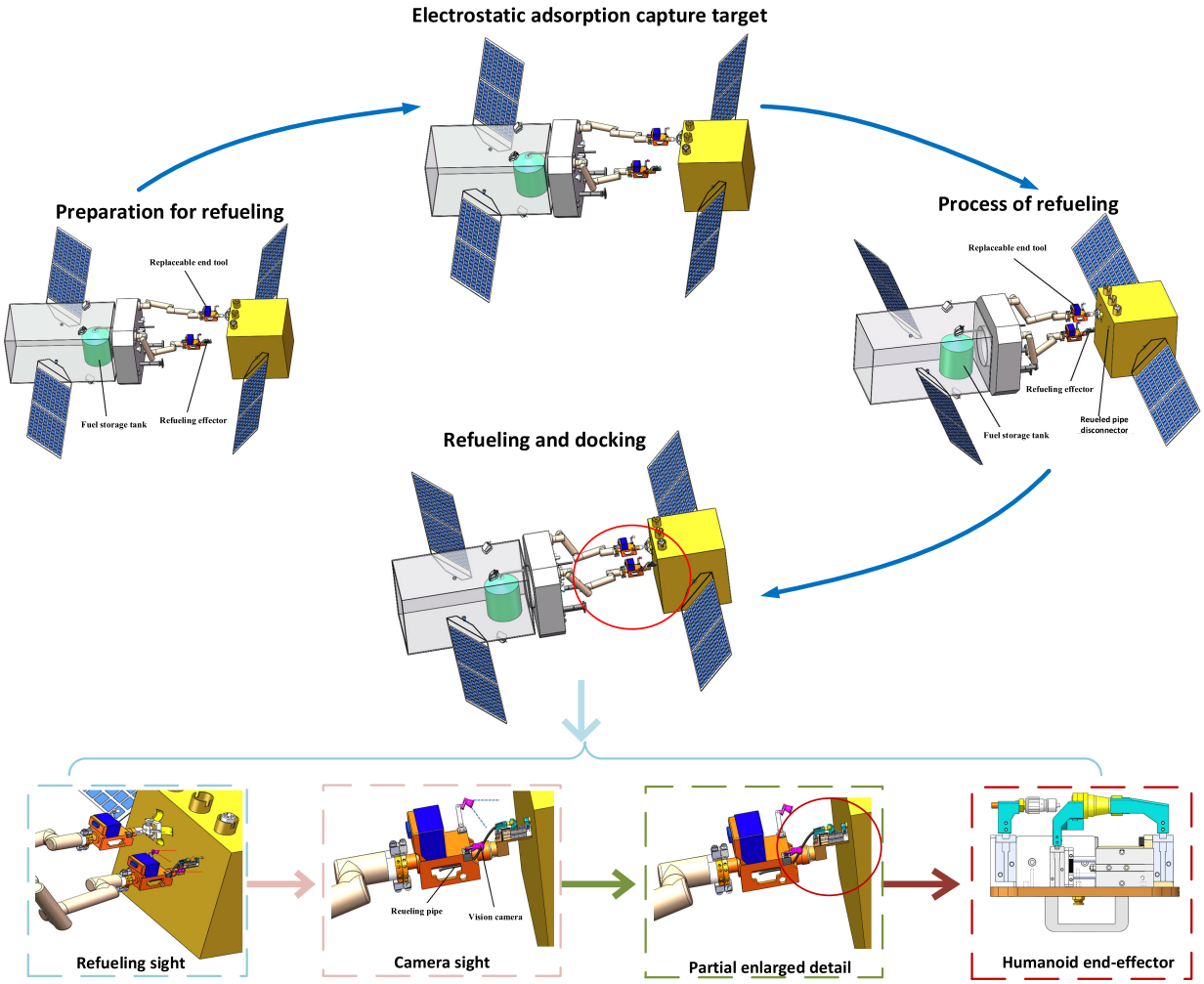

FIGURE 1. On-orbit robotic refueling mission plan.

the target aircraft. The target is then released and put into orbit.

At present, the space station on-orbit service is still rapidly developing, and on-orbit refueling operation has not been fully realized. During the process of an on-orbit robotic refueling mission, the pipe disconnectors are artificially docked, and the problems of a low efficiency and a long operation period are common. Using mechanism research from the perspective of bionics, this paper researched the kinematics of the upper limbs and hands of the human body in the manual docking process of pipeline quick disconnectors, analysed the redundant degrees of freedom in the manual docking process, and determined the configuration design scheme. Based on the bionics principle, this paper designed a new refueling tool that is mainly used to study the automatic docking problem of a straight-in type quick disconnector in the refueling system. In this paper, without changing the original structure of the quick disconnector, a five-degrees-of-freedom multifunctional end-effector imitating the human hand with a compact structure and a light weight was created, which can realize automatic docking of the quick disconnector in the pipeline. The quick disconnector docking in the refueling system is simplified from the original manual two-handed operation to a single-end-effector operation with a single mechanical arm. Compared with a dual-arm robot, a single-arm robot has the advantages of internal force sealing, a stable structure, a higher docking accuracy and a lower cost. The common rigid body contact collision dynamics problem is thus studied. The contact dynamics model between the ''quick disconnector and the robot end-effector'' is established by the equivalent spring damping model method. The experimental prototype was developed according to the structure of the end-effector to complete the construction of the refueling robot experimental platform. A simulation and experiment were conducted to verify the advantages and effectiveness of the structure.

The paper is organized as follows. The first section introduces the research background and the significance of an end-effector imitating the human hand and conducts a full investigation on the domestic and international research

results of on-orbit services and the research status of on-orbit robotic refueling mission systems. The scheme design and principle analysis of the on-orbit robotic refueling mission task are then introduced, laying the foundation for the introduction of the end-effector imitating the human hand. Section 2 demonstrates the method of manually docking the pipeline quick disconnector and analyses the mechanical structure and working principle of the pipeline quick disconnector. A structural analysis and the design of the end-effector are conducted by using the operation mechanism of an artificial hand. Section 3 analyses the modelling method of a typical contact force model according to the contact collision problem of the robot end-effector when clamping the pipe quick disconnector. Section 4 develops an experimental prototype of the refueling robot end-effector, installs an experimental prototype of the end-effector to form the refueling robot's experimental platform, and performs a structural analysis and test verifications. Section 5 summarizes the research work done in this paper and introduces future development prospects.

II. STRUCTURAL DESIGN OF AN END-EFFECTOR IMITATING A HUMAN HAND

The design of the end-effector is the basis and key to studying the entire grasping and docking process of the refueling robot. The structural design directly affects the gripping result of the refueling robot and the success rate of the quick disconnector docking. This section will first study the kinematics and working principle of the upper limbs in the manual docking process of the pipeline quick disconnector and then analyse the redundant degrees of freedom in the manual docking process. It will also briefly analyse the mechanical structure and working principle of the quick disconnector. Then, this section will focus on the introduction of the structure and working principle of the end-effector. Finally, using the statics analysis of the key components in the end-effector, the strength and stiffness of the designed structure will be judged to meet the actual requirements.

A. PROCESS OF MANUAL DOCKING

At present, the space station on-orbit service is still developing rapidly, on-orbit refueling operation has not been fully realized. Most spacecraft refueling missions require manual docking operations. During the process of an on-orbit robotic refueling mission, the pipe disconnectors are artificially docked, and the problems of a low efficiency and a long operation period are common. The docking of the quick disconnector with the gas valve and the liquid valve is realized by manual docking. The manual docking method of the pipeline quick disconnector is as shown in Figure 2.

The manual docking method is mainly divided into four steps. First, hold the quick disconnector's male disconnector with the left hand and move it to the vicinity of the female disconnector, as shown in Figure 2 (a). Second, use the thumb and index finger of the right hand to pull the sliding sleeve lock on the left side of the female disconnector to the right,

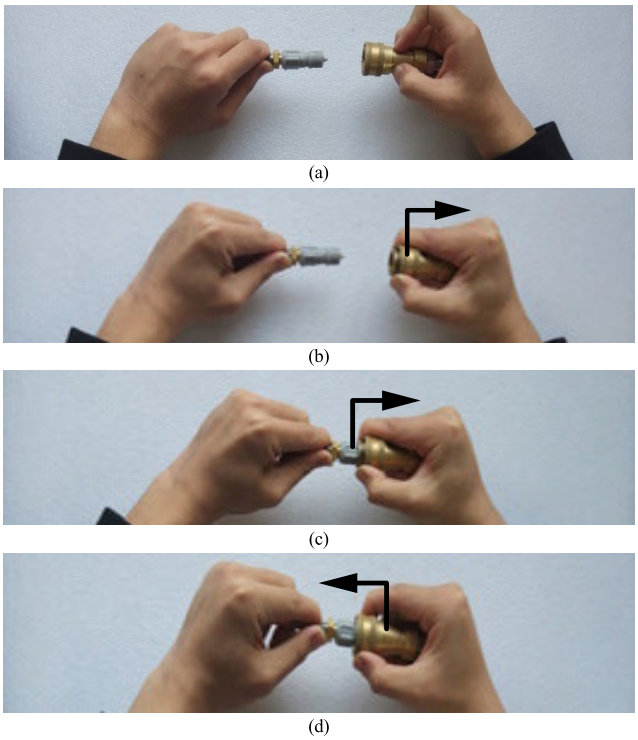

FIGURE 2. Quick disconnector manual docking process.

as shown in Figure 2 (b). Third, move the male disconnector along the axis of the female disconnector, so that the locking ball inside the female disconnector falls into the annular concave of the male disconnector in the slot, as shown in Figure 2 (c). Fourth, loosen the sliding sleeve lock held by the right thumb and forefinger. The sliding sleeve then returns to the original position by the spring force, restricting the locking ball from moving along the radial direction, as shown in Figure 2 (d). Thus, manual docking of the quick disconnector has been completed.

To complete the process from manual grasping to manual docking, many disconnectors from the upper limbs of the human body are needed. As shown in Figure 3, the kinematic model of the human upper limbs can be equivalent to the link model with 27 degrees of freedom. There are 7 degrees of freedom from the shoulder disconnector to the wrist disconnector, among which are the shoulder disconnector, which is a ball and socket disconnector with 3 degrees of freedom, the elbow disconnector, which has 2, and the wrist disconnector, which also has 2. There are still 20 degrees of freedom in the disconnectors of the human hands after removing the wrist disconnectors.

B. THE STRUCTURE AND WORKING PRINCIPLE OF THE QUICK DISCONNECTOR

The quick disconnector is an important component of the liquid refueling circuit. The success of its docking directly affects the transmission of liquid fuel in the refueling system.

The internal structure of the quick pipeline disconnector is mainly composed of an O-type sealing ring, ball,

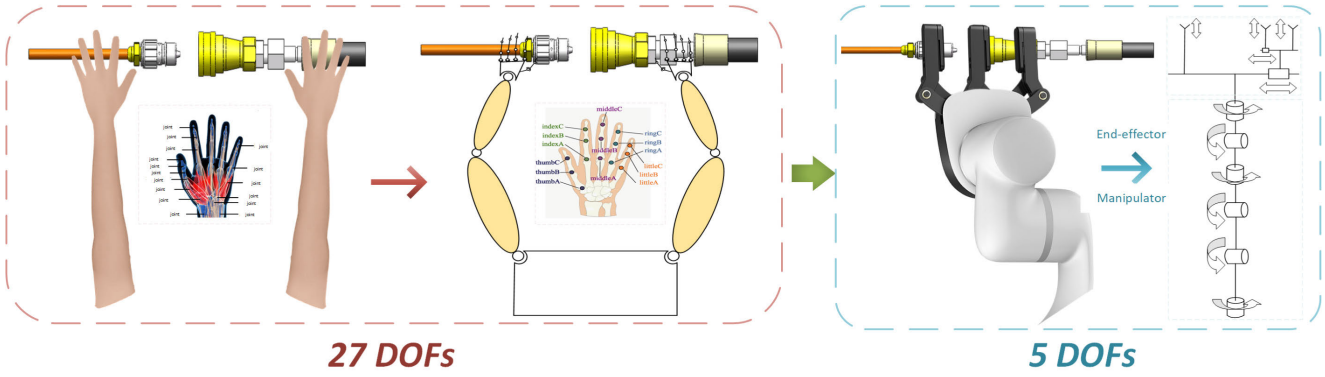

FIGURE 3. Left: Manual docking concept map. Right: Machine docking instead of manual docking: concept diagram for one-arm robot docking.

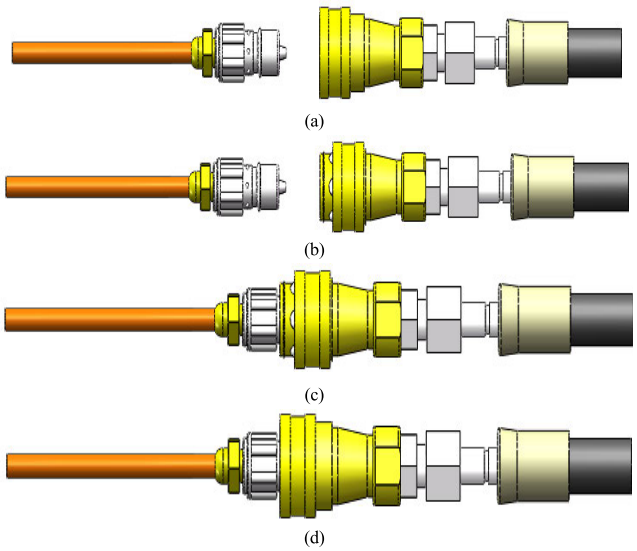

FIGURE 4. The working principle of the quick disconnector.

sliding sleeve and reset spring. The working principle of the fast disconnector is shown in Figure 4. The realization of the docking process can be divided into the following four steps:

When the pipeline is connected, first move the male disconnector to the vicinity of the female disconnector, as shown in Figure 4 (a), and then open the sliding sleeve lock at the front end of the female disconnector, as shown in Figure 4 (b). Second, move the male disconnector forward to make the locking ball fall into the annular groove of the male disconnector for locking, as shown in Figure 4 (c). Due to the axial limit of the ball, the self-sealing valves of the disconnectors on both sides interact with one another to make the compression spring move and compress, as shown in Figure 4 (d), so that the pipeline is connected.

C. STRUCTURAL DESIGN AND WORKING PRINCIPLE OF THE END-EFFECTOR IMITATING HUMAN HAND

According to the manual docking operation process, the end-effector of the automatic refueling robot was designed by imitating the manual operation method.

First, the driving method of the end-effector is determined. Pneumatic driving uses air pressure as the medium to realize the transmission of energy and signals, and a general pneumatic device has the advantages of a simple structure, convenient installation and disassembly quick action. Therefore, the end-effector uses pneumatic drive.

After determining the driving mode adopted by the end-effector, the SolidWorks software package is used to design the other connecting parts in the end-effector, and the parts and the cylinder model are matched to obtain the refueling robot end-effector mode, as shown in Figure 5 (a).

As can be observed from Figure 5 (b), the end-effector has a total of five degrees of freedom, which are provided by three parallel open-close type clamping cylinders and two telescopic type double-axis cylinders. The cylinders in the end-effector are all installed vertically. They have a compact structure, small volume and light weight, which can meet the requirements of the end load of the mechanical arm. Since the fixed telescopic cylinder has a large impact during ventilation, a guide groove is added to the bottom plate of the end-effector, which can restrict the left and right swing of the telescopic rod of the fixed telescopic cylinder to a certain extent, is conducive to the movement of the movable support plate in the horizontal direction, and reduces the docking error of the pipe disconnectors. The fingers of the end-effector are independently designed according to the external contour characteristics of the quick disconnector and the relative positions of the driving cylinder and the quick disconnector. The three pairs of effector fingers do not have the same height, but they can ensure that the axis lines of the male and female disconnectors are in the same line after clamping the fast disconnectors.

The working principle of the end-effector is as follows: first, effector A is allowed to hold the left end of the male disconnector, and at the same time, effectors B and C are allowed to grip the sliding sleeve lock on the female disconnector and the right end of the female disconnector, respectively. Then, the telescopic cylinder rod is driven to the right to retract, and the sliding sleeve lock is unlocked. Second, the fixed telescopic cylinder is ventilated, so that the telescopic rod is retracted to the left, driving clamping jaw C and the

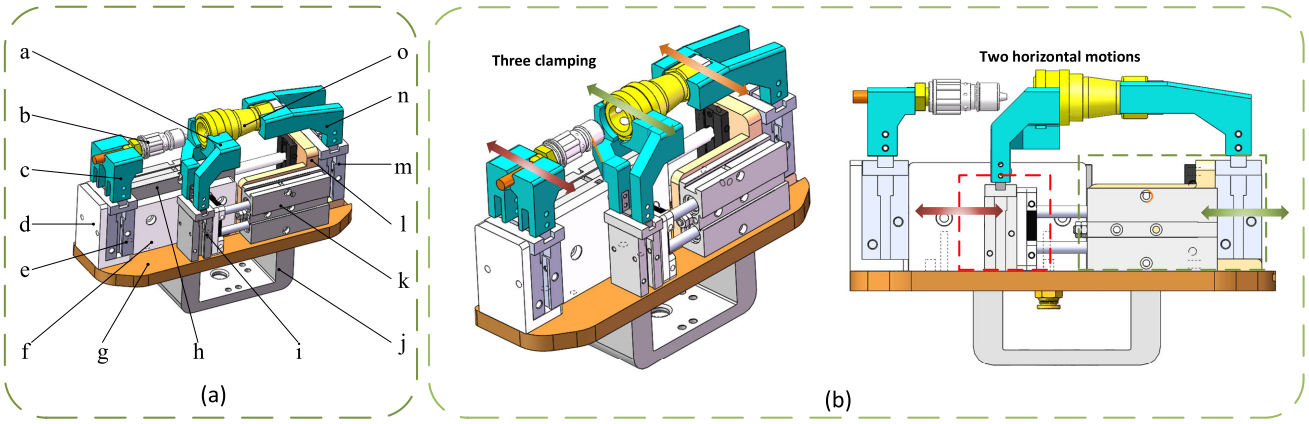

FIGURE 5. (a) End-effector structure (a. effector B, b. male pipe disconnector, c. effector A, d. cylinder support plate, e. cylinder of effector A, f. fixed plate of cylinder, g. bottom plate, h. fixed telescopic cylinder, i. cylinder of effector B, j. flange, k. moving telescopic cylinder, l. movable support plate, m. cylinder of clamping jaw C, n. clamping jaw C, and o. female pipe disconnector). (b) Model design of 5-DOF end-effector with artificial hand operation.

TABLE 1. Clamping cylinder selection.

Type	Pressure range	Stroke	Weight	Clamping force
TN16X10	0.1-1Mpa	20mm	150g	350N
TN16X40	0.1-1Mpa	80mm	375g	350N
MHZ2-10S	0.1-0.7Mpa	8mm	120g	36N
MHZ2-16S	0.1-0.7Mpa	12mm	400g	48N

female disconnector to move to the left, thus making the reset spring inside the male disconnector and female disconnector push each other open. Therefore, the liquid medium in the male pipeline disconnector can flow to the female pipeline disconnector.

The pneumatic effector required for the design of the end-effector are selected. The air cylinder pressure range, weight, stroke, the clamping force of the cylinder and other aspects are mainly selected. The model of the pneumatic effector is presented in Table 1.

D. STATICS ANALYSIS OF THE EFFECTOR FINGER IMITATING THE HUMAN HAND

Due to the limited load at the end of the manipulator, it is necessary to conduct a weight reduction design for some supporting plates on the end-effector and to ensure the rationality of the structural stress. Finite element software can be used to calculate the parts under the load state, so the stress and displacement cloud map can be obtained, and the dangerous area of the structure and the area with a large rigidity margin can be analysed. Through the typical load-bearing design, a ribbed plate or load-bearing cylinders is added to the dangerous area. For an area with redundant stiffness, a redundant mass can be appropriately reduced or hollowed out, and the ratio of the bearing capacity to weight can be increased to complete the optimal design of the structure. The finger of the end-effector is one of the core components for completing the automatic docking of the quick pipeline disconnector. The movement of the effector finger is realized by pneumatic driving, wherein the strength and rigidity of the effector fingers have a great influence on the effector stability of the quick disconnector and the success rate of the docking. Therefore, this section uses the Ansys/Workbench software package to perform a mechanical analysis on each finger of the effector.

TABLE 2. Material properties.

Material	Yield Strength	Elastic Modulus	Poisson's Ratio
Aluminum Alloy 7075	505MPa	71.7GPa	0.33

The steps for the static analysis of the end-effector fingers are as follows: first, the 3D model file established by SolidWorks is imported into the Workbench platform.The material of the end-effector finger is set to aluminium alloy 7075, and the basic properties of the material are reported in Table 2. When the material and other properties are set, the grid-division of the effector finger is conducted.

After the mesh is divided, the fixed constraint and the force load are added to the effector finger. It is concluded that the force needed to open the locking spring is 100 N, so the force load to the effector is 100 N. A fixed constraint is added to the mounting bolt holes of effector. The displacement and stress cloud diagrams of the effector fingers are obtained through the solver analysis, as shown in Figure 6 (a)-(b).

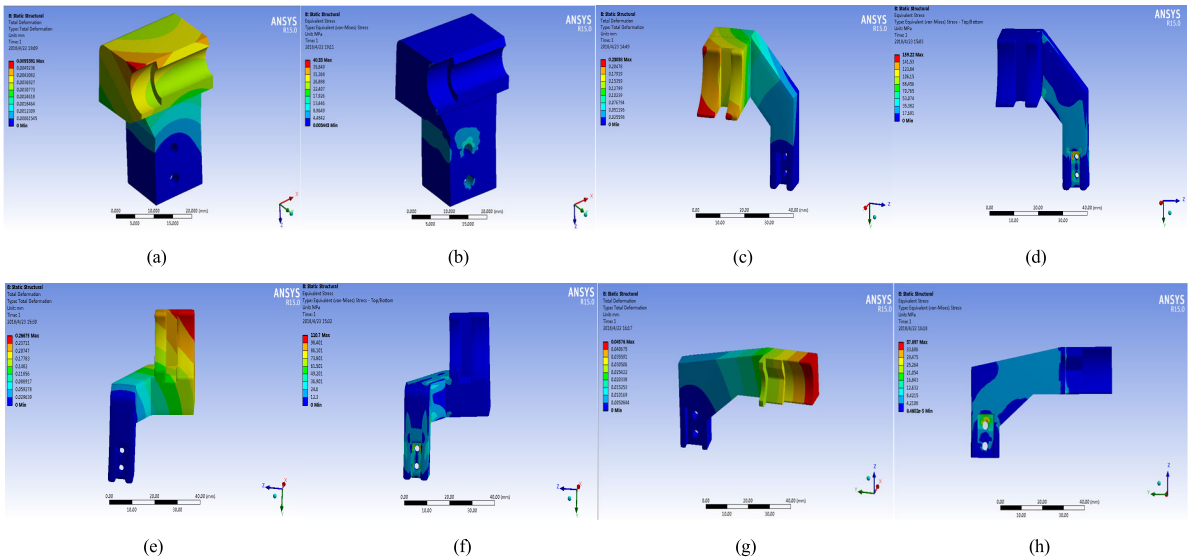

FIGURE 6. (a)-(b) Static analysis of effector finger A. (c)-(d) Static analysis of effector finger B (right finger). (e)-(f) Static analysis of effector finger B (left finger). (g)-(h) Static analysis of effector finger C.

From the analysis results, it can be concluded that the maximum stress of effector finger A is 40.33 MPa, which is far from the yield strength of 505 MPa of aluminium alloy 7075, with no plastic deformation occurring. The maximum displacement in the X direction is 4.83e-003 mm, the maximum displacement in the Y direction is 1.3423e-003 mm, and the maximum displacement in the Z direction is 1.2884e-003 mm. Therefore, it is understood that the deformation of effector finger A is very small, and the rigidity is sufficient.

Similarly, a fixed constraint and force load are applied to effector finger B, and then a displacement cloud map and a stress cloud diagram of effector finger B are obtained, as shown in Figure 6 (c)-(d). The maximum stress of effector finger B (right finger) is 159.22 MPa, the displacement in the X direction is 0.15165 mm, the displacement in the Y direction is 1.5845e-002 mm, and the displacement in the Z direction is 0.19676 mm.

Figure 6 (e)-(f) shows the stress and displacement cloud diagrams of effector finger B (left finger). It can be observed from the figure that the maximum stress is 110.7 MPa, the displacement in the X direction is at most 0.1307 mm, the displacement in the Y direction is at most 6.362e-003 mm, and the displacement in the Z direction is at most 0.22106 mm.

A fixed constraint and a force load are applied to effector finger C to obtain the displacement and stress cloud diagrams of effector finger C, as shown in Figure 6 (g)-(h). According to the figure, the maximum stress on the left finger of effector finger C is 37.897 MPa, the maximum displacement in the X direction is 2.5894e-003 mm, the maximum displacement in the Y direction is 1.8547e-002 mm, and the maximum displacement in the Z direction is 1.6578e-002 mm.

Through a simple statics analysis, it can be determined that the maximum displacement and maximum stress of each effector finger are relatively small, which indicates that the designed structure of the end-effector can meet the strength and rigidity requirements of a quick disconnector in grasping and docking.

III. CONTACT DYNAMICS ANALYSIS OF THE REFUELING ROBOT

The contact collision problem of multi-body systems is common in engineering practice, which will have a huge impact on the design and analysis of the mechanical system. In the near future, space robots will undertake an increasing number of tasks, and the difficulty will increase gradually. Contact collision will inevitably occur during the completion of the mission, such as on-orbit maintenance, on-orbit robotic refueling and on-orbit assembly on the space station. The contact and collision between the end of the manipulator and the target object is thus a problem that cannot be ignored. The contact and collision at the end of the robot will directly affect the magnitude and posture of the end force of the robot. This section focuses on the external contact collision of robots. The study of external collision dynamics helps to improve the control accuracy of the robot and the accuracy of the trajectory planning.

First, this section analyses the universality and significance of contact collision in engineering. Second, it introduces several commonly used contact force models, including the generalized contact force model, a nonlinear Hertzian contact model, an equivalent spring damping model, etc. The contact spring dynamics model of the effector and the quick disconnector is established by the effective spring damping model method. Finally, a virtual prototype test platform is built using the Adams software package to simulate the collision process between the effector and the quick disconnector, and the contact collision simulation results are analysed to obtain the maximum contact force during the collision, as well as the

law diagram of the acceleration, velocity and displacement of the centroid of the effector finger versus time.

A. CONTACT COLLISION PROBLEM IN OOS

The key part of the dynamics modelling method used in OOS is contact dynamics (including low-speed impact dynamics). The early application of contact dynamics in space robots was reported in [37], [38], where the contact force was modelled as an impulse function under the assumption of a point contact situation. Therefore, Ma *et al.* [39] developed a universal contact dynamics modelling and simulation system. They further developed a model reduction technique to improve the high fidelity efficiency, but contact dynamics simulations are usually very time consuming [40]. Shibili *et al.* [41] proposed a contact dynamics analysis method that regarded the generalized binding force between the end-effector of the space robot and the target satellite as an internal force rather than an external force. Nenchev and Yoshida [42] also discussed the contact dynamics modelling and control issues of a space manipulator. Ma *et al.* [43] developed a control strategy for implementing high-fidelity contact dynamics simulation of robot-based new hardware-in-the-loop rendezvous and docking simulations. Abiko *et al.* [44] introduced a contact dynamics simulation method to capture distant floating targets through a space manipulator with a clue-type end effector. Uyama *et al.* [45] presented an experimental evaluation of contact/impact dynamics between space robots and tumbling objects. Sawada *et al.* [46] focused on the contact dynamics of the end-effector of the manipulator and the grab fixing device of the target satellite. A review of common contact dynamics modelling techniques can be found in [47].

B. CONTACT FORCE MODELLING METHOD

The initial analysis of the multi-rigid-body system collision problem is based on the following assumptions: (1) The collision objects are all rigid bodies. (2) The collision process is extremely short, and considering the action time and action process is not necessary. (3) The contact and collision position is regarded as a point contact, and the contact position of the whole collision link remains unchanged. (4) The change in the motion state of the rigid body is judged according to the change in the impulse before and after the collision.

1) GENERALIZED CONTACT KINEMATICS MODEL

First, the generalized contact kinematics between two rigid bodies subjected to an oblique eccentric impact is described. Figure 7(a) shows the state in which objects 1 and 2 are separated at an absolute speed $\dot{r}_1$ and $\dot{r}_2$, respectively. The potential contact points are indicated by P1 and P2.

The vector connecting the two potential contact points P1 and P2 can be expressed as follows:

$$\mathbf{d} = \mathbf{r}_2^P - \mathbf{r}_1^P \tag{1}$$

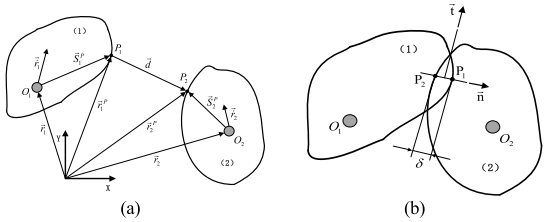

FIGURE 7. (a) Two objects in a separated state. (b) Two objects in contact (indentation δ).

where r_1^P and r_2^P are the descriptions in the global coordinates relative to the inertial reference system, expressed as follows:

$$\mathbf{r}_k^P = \mathbf{r}_k + \mathbf{A}_k \mathbf{s}'^P_k \quad (k = 1, 2) \tag{2}$$

where $\mathbf{r}_1^P$ and $\mathbf{r}_2^P$ respectively represent the position vectors of objects 1 and 2 in the global coordinate system, and $\mathbf{s}'^P_1$ and $\mathbf{s}'^P_2$ are the respective contact point coordinate components related to the local coordinate system. The plane rotation matrix $\mathbf{A}_k$ is represented as follows:

$$\mathbf{A}_k = \begin{bmatrix} \cos\phi_k & -\sin\phi_k \\ \sin\phi_k & \cos\phi_k \end{bmatrix} \quad (k = 1, 2) \tag{3}$$

As shown in Figure 7(b), the normal vector of the contact plane can be expressed as follows:

$$\mathbf{n} = \frac{\mathbf{d}}{d} \tag{4}$$

The length of the vector $\mathbf{d}$ is as follows:

$$d = \mathbf{n}^T \mathbf{d} \tag{5}$$

Since the above assumption does not cover all the situations that may occur, the minimum distance condition given by equation (5) is not sufficient for finding the possible contact points between the contact bodies. Therefore, the contact point is defined as the contact position corresponding to the maximum indentation, that is, the maximum relative deformation point measured along the normal direction. Therefore, the three geometric conditions of contact can be defined as follows:

(1) The distance between the potential contact points is given by the vector corresponding to the minimum distance.

(2) Vector $\mathbf{d}$ is collinear with the vector $\mathbf{n}_1$.

(3) The normal vectors $\mathbf{n}_1$ and $\mathbf{n}_2$ are collinear at the potential contact point.

This is described in mathematical language as follows:

$$\mathbf{n}_2 \times \mathbf{n}_1 = \mathbf{0} \tag{6}$$

$$\mathbf{d} \times \mathbf{n}_1 = \mathbf{0} \tag{7}$$

Equations (6) and (7) are nonlinear equations with two unknowns. After determining the location of the contact collision points, the corresponding contact indentation δ can be solved as follows:

$$\delta = \sqrt{\mathbf{d}^T \mathbf{d}} \tag{8}$$

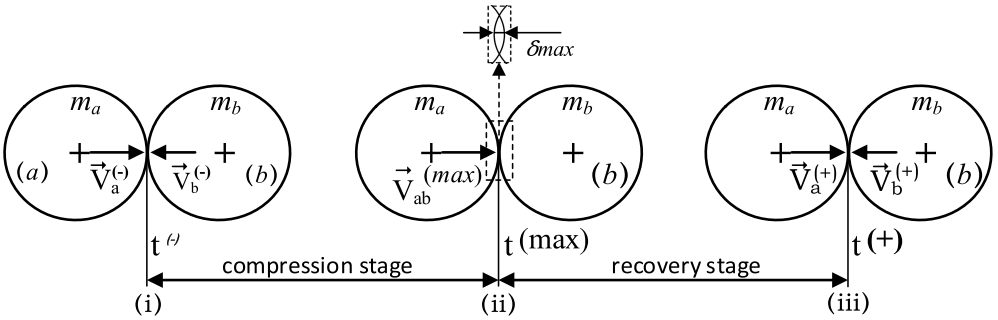

FIGURE 8. The process of a contact collision between two spheres.

Equation (2) is differentiated with respect to time to obtain the velocity of the contact point in the global coordinate system:

$$\dot{\mathbf{r}}_k^P = \dot{\mathbf{r}}_k + \dot{\mathbf{A}}_k \mathbf{s}'^P_k \quad (k = 1, 2) \tag{9}$$

The relative normal velocity can be solved by projecting the velocity of the contact point into the direction perpendicular to the contact plane, i.e.

$$v_N = \dot{\delta} = \mathbf{n}^T \left(\dot{r}_2^P - \dot{r}_1^P \right) \tag{10}$$

The above description is limited to convex rigid bodies with smooth surfaces near the potential contact points. In fact, the method can be extended to more generalized contact geometries as long as the common tangent plane of the two contact bodies is unique.

2) NONLINEAR HERTZIAN CONTACT MODEL

The most common contact force model is based on Hertz's work, which uses elastic theory to represent collisions between two isotropic material spheres. It is worth noting that Hertz contact theory is limited to frictionless surfaces and completely elastic solids. Hertz's law relates the contact force to the nonlinear power function of the deformation, which can be expressed as follows:

$$F = K\delta \tag{11}$$

where K is the generalized stiffness parameter, δ represents the same relative penetration or indentation, n = 3/2, and the contact force distribution is in the form of a parabola.

The generalized stiffness parameter K depends on the properties of the material and the shape of the contact surface. For contact between two spheres, the generalized stiffness parameters are functions of spheres 1 and 2 and the material properties as follows:

$$K = \frac{4}{3\left(\sigma_1 + \sigma_2\right)} \sqrt{\frac{R_1 R_2}{R_1 + R_2}} \tag{12}$$

The material parameters $\sigma 1$ and $\sigma 2$ in the equation can be calculated using the following equation:

$$\sigma_l = \frac{1 - \nu_l^2}{E_l}, \quad (l = 1, 2) \tag{13}$$

where ν_l is the Poisson's ratio of the sphere and E_l is the Young's modulus.

For the contact of the sphere and plane type, the generalized stiffness parameter can be expressed as follows:

$$K = \frac{4}{3\left(\sigma_1 + \sigma_2\right)} \sqrt{R_1} \tag{14}$$

It should be noted that the object contact surface is concave with a negative radius, such as mechanical disconnector clearance, and convex with a positive radius.

3) EQUIVALENT SPRING DAMPING MODEL

Broadly speaking, the contact process can be divided into two distinct stages, namely, the compression stage and the recovery stage, which begins when the two spheres in contact and ends when the maximum deformation is reached. During this stage, the relative velocity of the contact points on the two bodies in the normal contact direction gradually decreases to zero. When the contact deformation reaches the maximum, the compression phase ends. If energy dissipation is not considered, the normal contact force at this time should be the maximum. Instead, the recovery phase begins at this point and ends when the two spheres separate from one another.

As shown in Figure 8, there are two distinct phases of the direct central contact between two solid spheres.

where m_a and m_b respectively represent the masses of sphere (a) and sphere (b), $v_a^{(-)}$ and $v_a^{(+)}$ respectively represent the velocity of the sphere (a) before and after the collision, and $v_b^{(-)}$ and $v_b^{(+)}$ respectively represent the velocity of the sphere (b) before and after the collision. At the end of the compression phase, the two spheres move at a common instantaneous velocity, represented by the variable $v_{ab}^{(\max)}$.

The equivalent spring damping model considers that the collision process is no longer a transient process and regards the contact force as a unique force. A spring damping model is used to equivalently replace the contact force, and the continuous force-displacement relationship is used to address the collision between two objects. As shown in Figure 9, it is assumed that the radius of the curvature of the contact points of the two rigid bodies are r_a and r_b, respectively, and the normal direction **n** to the contact surface is positive. Considering material damping, the generalized contact force

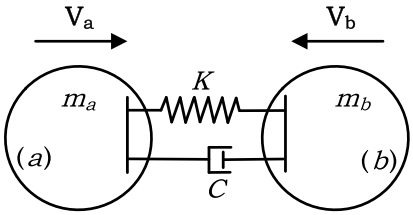

FIGURE 9. Two objects in contact (indentation δ).

can be expressed as follows:

$$\mathrm{F} = \mathrm{K}\delta^{\mathrm{n}} + \mathrm{D}\dot{\delta} \tag{15}$$

where K is the generalized stiffness parameter, δ represents the distance of the relative penetration or penetration, n = 3/2, the contact force distribution is in the form of a parabola, D represents the damping coefficient of the damper, $D = \xi\delta^n$, and $\dot{\delta}$ indicates the relative normal velocity between the contact points.

C. CONTACT DYNAMICS MODELLING OF AN EFFECTOR IMITATING A HUMAN HAND

By comparing the three methods of contact force modelling introduced in the previous section, it can be observed that the generalized contact force model is limited to a convex rigid body with a smooth surface near the potential contact point or the unique common tangent plane of the two contact bodies. The nonlinear Hertzian contact model is limited to frictionless surfaces and completely elastic solids, while the equivalent spring damping model has fewer constraints and is conveniently applied. Therefore, the equivalent spring damping method is used to establish the mathematical model of the contact collision between the effector and the quick disconnector.

In fact, there is always normal deformation and tangential deformation in the contact position during the collision, and the magnitude of the deformation is related to the local material properties and external forces on the collision object. The two contact collision objects are the effector finger and the quick disconnector. In the global coordinate system, point P1 on the effector finger and point P2 on the quick disconnector are potential contact points. A local coordinate system is established at point P1 {P1 and n1, t1}, where the unit normal vector in the n1 direction is $\mathbf{n}'_1$, the unit tangential vector in the t1 direction is $\mathbf{t}'_1$, and the positive direction of the normal vector is defined outward, as shown in Figure 10.

According to the relative displacement S between two adjacent points P1 and P2, the shortest normal relative distance Sn between the effector and the quick disconnector can be determined as follows:

$$\mathbf{S}_n = \mathbf{S} \cdot \mathbf{n}'_1 = (\mathbf{r}_2 - \mathbf{r}_1) \cdot \mathbf{n}'_1 \tag{16}$$

where $\mathbf{r}_1$ and $\mathbf{r}_2$ is the vector of the origin O to the contact points P1 and P2 in the global coordinate system XOY.

According to the positive and negative of the normal direction of the relative distance, Sn determines whether

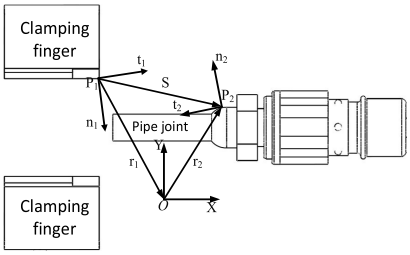

FIGURE 10. Local coordinate system for a rigid body contact.

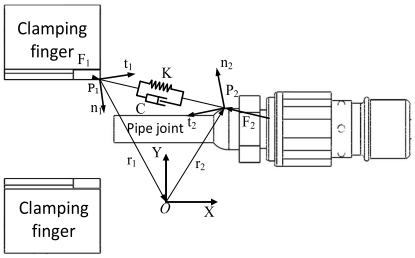

FIGURE 11. Contact impact force model of the effector.

there is contact, if Sn > 0, it means that the effector finger and the quick disconnector are not in contact. If Sn = 0, it means that the effector finger and the quick disconnector just touch. If Sn < 0, it means that the effector finger and the quick connector are embedded with each other.

Since $\mathbf{n}'_1$ is a unit normal vector, its length is constant, so $\mathbf{n}'_1$ is orthogonal to $\dot{\mathbf{n}}'_1$, because the relative displacement S between two adjacent points P1 and P2 is in the direction of $\mathbf{n}'_1$, so $\mathbf{S} \cdot \mathbf{n}'_1 = 0$. Therefore, the relative velocity between the nearest points along the normal direction is as follows:

$$\dot{\mathbf{S}}_{\mathrm{n}} = \dot{\mathbf{S}} \cdot \mathbf{n}'_1 + \mathbf{S} \cdot \dot{\mathbf{n}}'_1 = \dot{\mathbf{S}} \cdot \mathbf{n}'_1 = \left(\mathbf{y}_{OP_1} - \mathbf{y}_{OP_2}\right) \cdot \mathbf{n}'_1 \tag{17}$$

The generalized coordinates can be expressed as follows:

$$\begin{aligned} \dot{\mathbf{S}}_n &= \left(\mathbf{J}_{TP_2} \cdot \dot{\mathbf{y}} + \mathbf{v}_{P_2} - \mathbf{J}_{TP_1} \cdot \dot{\mathbf{y}} + \mathbf{v}_{P_1}\right) \cdot \mathbf{n}'_1 \\ &= \left(\mathbf{J}_{TP_2} - \mathbf{J}_{TP_1}\right) \cdot \mathbf{n}'_1 \cdot \dot{\mathbf{y}} + \left(\mathbf{v}_{P_2} - \mathbf{v}_{P_1}\right) \cdot \mathbf{n}'_1 \\ &= \mathbf{w}_n \cdot \dot{\mathbf{y}} + \mathbf{k}_n \end{aligned} \tag{18}$$

where $\mathbf{w}_{\mathrm{n}}$ is the projection of the generalized velocity in the normal direction, $\mathbf{w}_n = \left(\mathbf{J}_{TP_2} - \mathbf{J}_{TP_1}\right) \cdot \mathbf{n}'_1$, $\mathbf{k}_{\mathrm{n}}$ is the normal projection of the relative velocity in an unsteady system, $\mathbf{k}_n = \left(\mathbf{v}_{P_2} - \mathbf{v}_{P_1}\right) \cdot \mathbf{n}'_1$, $\mathbf{J}_{TP_1}$ and $\mathbf{J}_{TP_2}$ represent the Jacobian matrix of the contact points P1 and P2, $\mathbf{v}_{P_1}$ and $\mathbf{v}_{P_2}$ indicate the relative velocity of contact points P1 and P2, respectively, and $\mathbf{y}$ indicates the generalized positional coordinate.

The equivalent spring damping model method is used to establish the dynamic model of the contact collision between the effector and the quick disconnector. The mechanical model is shown in Figure 11. The collision force is mainly caused by the local deformation near the contact point. Therefore, the penetration distance and the penetration speed between the two objects are used as the independent variables that cause the collision force to change. The size of the collision force F between the griper and the quick disconnector

can be obtained from equation (19), that is,

$$F = K\delta^{n} + D\frac{d\delta}{dt} \tag{19}$$

where K is the local contact stiffness at the contact point, D is the local damping coefficient at the contact point, δ is the contact deformation distance, $\delta = \delta(t) = \int \dot{S}_n dt$, $\frac{d\delta}{dt}$ is the normal relative velocity between the contact points, and n is the force exponent. In the Hertz contact problem, n = 3/2.

D. CONTACT DYNAMICS SIMULATION ANALYSIS OF AN EFFECTOR IMITATING A HUMAN HAND

This section will use Adams software to build a virtual prototype simulation experiment platform and use the Impact function (the model uses the equivalent spring damping model) to analyse the contact collision problem between the effector and the quick disconnector.

To facilitate the simulation operation of Adams software, SolidWorks is used to simplify the 3D model before importing the model of the effector and quick disconnector. Then, the corresponding parameters for each component are added according to the material actually used by the rigid body. To more accurately simulate the actual motion of the rigid body, the influence of friction must be considered when adding motion pairs and constraints to the motion disconnectors. Therefore, the static friction coefficient and dynamic friction coefficient in the rotating pair are set to 0.25 and 0.2, respectively. In addition, in order to simulate the external contact of the quick disconnector, a spring system with structural damping is added to the effector in the simulation system. The stiffness coefficient is set to 100 N/mm, and the damping ratio is set to 10 N · s/mm.

After adding the disconnector motion pairs and constraints, the contact relations between the effector fingers and quick disconnectors are added. According to the material properties of the effector and the quick disconnector, the parameters are set as follows. The local contact stiffness K = 3.5 × 104 N/mm, and the contact force index e = 3/2. The contact point damping coefficient D = 28 N·s/mm, the contact point embedding distance d = 0.1 mm, the static friction coefficient of the coulomb friction force $\mu s = 0.25$, and the dynamic friction coefficient of the coulomb friction force $\mu = 0.2$.

After the virtual prototype test platform is built, the virtual prototype effector is given a driving force to enable the effector to hold the quick disconnector. After the end of the simulation, the contact force between the effector and the quick disconnector is measured.

The results shown in Figure 12 (a) were obtained via Adams post-processing. It can be observed from the figure that between 0-0.0027 s, since the effector and the quick disconnector are not in contact, the contact force is 0. At 0.0027 s, the effector collides with the quick disconnector, and the collision force is 2377.81 N. After the collision is completed, the contact force tends to be stable such that the quick disconnector is clamped.

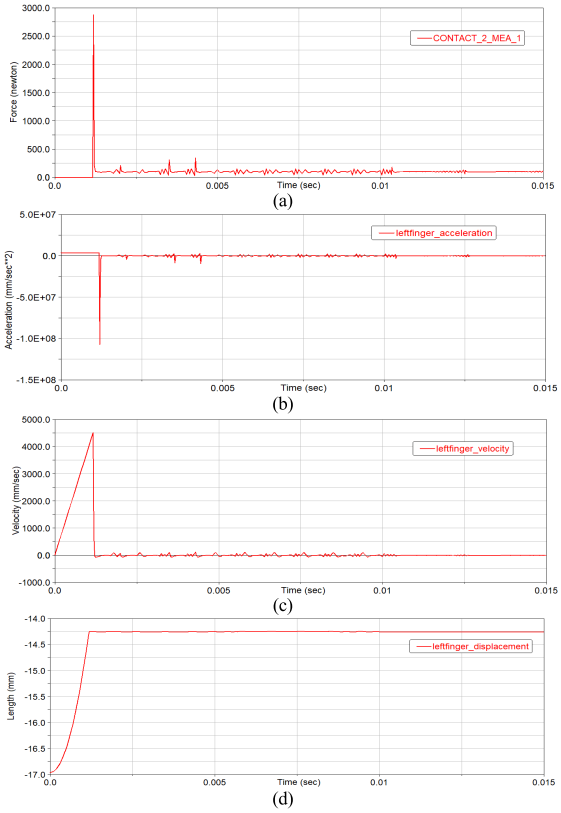

FIGURE 12. (a) The law of contact force changing with time. (b) Change law of the centroid acceleration of the effector finger. (c) Change law of the centroid speed of the effector finger. (d) Change law of the centroid displacement of the effector finger.

By measuring the centroid acceleration of the effector finger, it can be observed that the law of acceleration change and the change law of the contact force are similar, as shown in Figure 12 (b). In the interval of 0-0.0027 s, the acceleration is generated by the driving force that pushes the finger movement of the effector, which is a non-zero setting. At 0.0027 s, due to the instantaneous collision between the effector and the quick disconnector, the acceleration is determined by the resultant force of the collision force and the driving force. After the collision is completed, the acceleration goes to zero.

At the same time, the speed and displacement of the effector finger centroid are measured. Figure 12 (c) is the curve of the effector finger centroid velocity versus time, and Figure 12 (d) is the curve of the effector finger centroid displacement versus time. The figure shows that before the effector collides with the quick disconnector, the effector finger performs a uniform acceleration motion with an initial velocity of zero. When the collision occurs, the speed of the effector's finger changes suddenly from +2027 mm/s to -57 mm/s. After the collision is completed, the centroid velocity of the effector finger gradually becomes zero.

IV. GRASPING EXPERIMENT OF THE REFUELING ROBOT

To judge the completion of the grasping and docking task of the refueling robot more realistically, it must be tested experimentally. Therefore, an experimental prototype of the

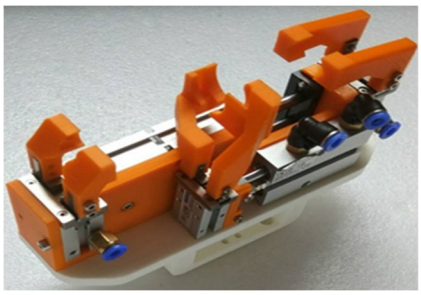

FIGURE 13. Experimental prototype of the end-effector.

end-effector of the refueling robot was developed, and an experimental platform of the refueling robot was built. The quick disconnector grasping experiment was conducted to verify the feasibility of the scheme. Based on the structural design and statics analysis of the end-effector, the experimental prototype of the end-effector of the refueling robot was developed, and the experimental platform of the refueling robot was built. Second, according to the working principle of the end-effector, the cylinder action sequence was analysed, and the schematic diagram of the pneumatic system was drawn. Finally, by debugging the end-effector control system and the communication between the manipulator controller and the upper computer, the refueling robot experiment was confirmed. It is verified by experiments that the refueling robot can grasp and dock the quick disconnector according to the pre-set trajectory.

A. EXPERIMENT PLATFORM OF THE REFUELING ROBOT

Based on the three-dimensional structure design of the end-effector, the static analysis of the end-effector in Section 2 and the contact dynamics analysis in Section 3, the principle prototype of the end-effector was machined. The main structure of the flange and the end-effector of the manipulator were processed and manufactured via 3D printing additive manufacturing technology. Figure 13 is a physical diagram of the end-effector principle prototype. The end-effector is mainly composed of three parallel open and closed pneumatic effectors and two horizontal telescopic cylinders. The fingers of the V-shaped mouth are installed above the effector for clamping the cylindrical quick disconnectors. The clamping centre of three effector fingers is the same height, which is convenient for docking of quick disconnectors.

The control system module of the end-effector is mainly composed of the PLC controller and the actuator solenoid valve. The controller is the PLC produced by the Mitsubishi Corporation, which is powered by 24 V DV power supply and has 24 input signal interfaces and 16 output signal interfaces. The solenoid valve adopts the middle-sealed three-position five-way solenoid valve of Yadeke Company, whose allowable pressure range is 0.15∼ 0.8 MPa. The program can control the energization and power-off time of each solenoid valve to achieve time sequential cylinders.

The terminal clamp control module is wired as shown in Figure 14. An intermediate relay is used between the PLC

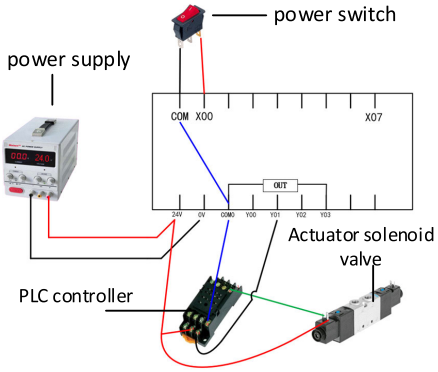

FIGURE 14. Wiring diagram of control system.

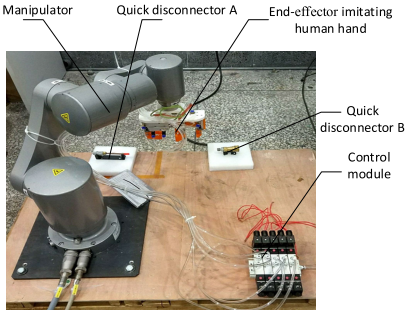

FIGURE 15. Experiment platform of the refueling robot.

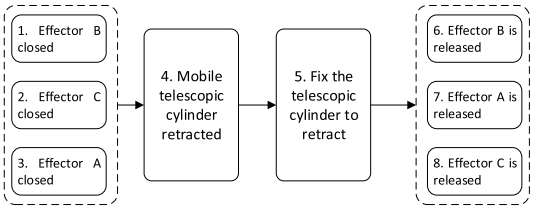

FIGURE 16. The cylinder working sequence.

controller and the solenoid valve to transmit the electronic control signals, because the intermediate relay can function as relay protection.

After production of the end-effector hardware system is completed, the end-effector is connected to the end of the manipulator through a flange, and the pneumatic pipeline is connected between the cylinder inlet of the end-effector and the solenoid valve to obtain the entire refueling robot test platform, as shown in Figure 15. The manipulator used in the experimental platform comes from the small manipulator SR4A produced by the Xinsong Company. The robot arm can realize the functions of carrying goods, loading and unloading, assembly, etc. and has abundant external interfaces for expansion. The terminal load is 4 kg, the repeated positioning accuracy is ±0.03 mm, and the maximum working radius is 580 mm.

B. ANALYSIS AND DESIGN OF THE END-EFFECTOR CONTROL SYSTEM

According to the working principle of the end-effector, the order of the cylinder movements can be sorted out, as shown in Figure 16. It can be observed from the figure

TABLE 3. I/O port allocation for PLC.

Input point	Input	Output point	Output
Start (SB1)	X0	Effector A clamping (YA1)	Y0
Stop (SB2)	X1	Effector B clamping (YA2)	Y1
Fixed telescopic cylinder left limit (SQ1)	X2	Effector C clamping (YA3)	Y2
Fixed telescopic cylinder right limit (SQ2)	X3	Fixed telescopic cylinder extension (YA4)	Y3
Mobile telescopic cylinder left limit (SQ3)	X4	Fixed telescopic cylinder retraction (YA5)	Y4
Mobile telescopic cylinder right limit (SQ4)	X5	Mobile telescopic cylinder extension (YA6)	Y5
		Mobile telescopic cylinder retraction (YA7)	Y6

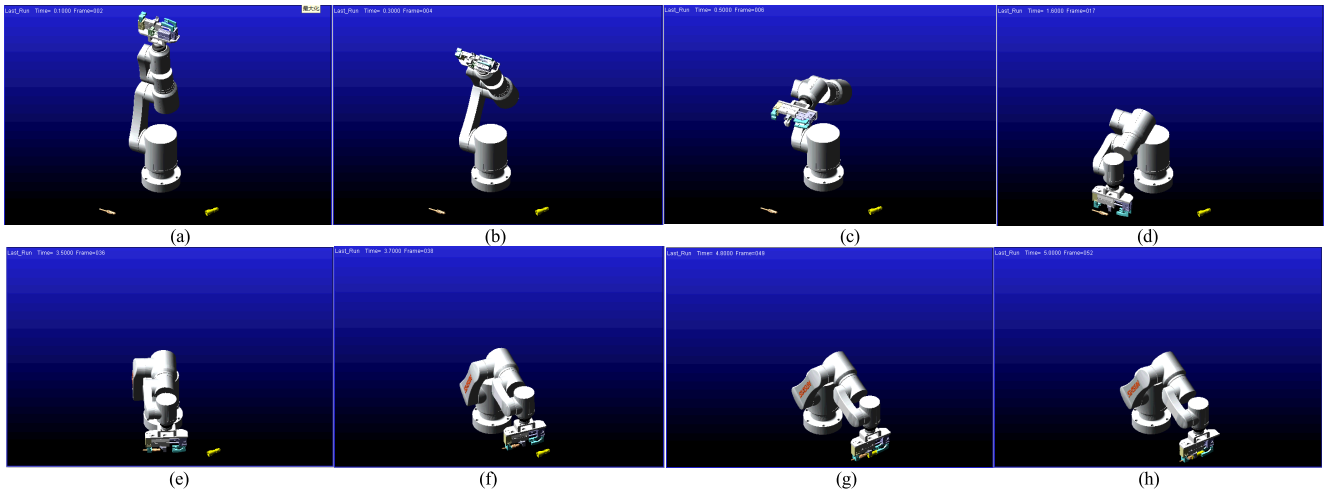

FIGURE 17. Adams grasping simulation experiment.

that the cylinder working sequence is as follows: energization → reset → start → effector B closed → effector C closed → effector A closed → mobile telescopic cylinder retracted → fix the telescopic cylinder to retract → effector B is released → effector A and effector C are released.

After the working sequence of the end-effector is clarified, the end-effector pneumatic transmission system is analysed and designed. The pneumatic system is mainly composed of pneumatic pumps, air source triplets, pneumatic circuit control valves and various executive cylinders. The pneumatic control components are selected from the relevant products in SMC and Yadeke. To make each cylinder run smoothly, a one-way speed regulating valve is separately installed in each pneumatic circuit. The cylinder type used for effector A and effector C is MHZ2-16S. The cylinder type used for effector B is MHZ2-10S. The cylinder type for the fixed telescopic cylinder is TN16x40. The cylinder model selected for the mobile telescopic cylinder is the Yadak TN16x10.

PLC is used to control the solenoid valve. The effector cylinder in the end-effector is a single-acting cylinder, so it can be controlled by a single-acting solenoid valve, and the telescopic cylinder is a double-acting cylinder controlled by a dual electronically controlled three-position five-way solenoid valve. According to the control requirements of the end-effector, the PLC control system has a total of 6 signal inputs and 7 signal outputs, wherein the specific functions of the input signal and the output signal are reported in Table 3. Therefore, the number of PLC input points should not be less than 6, and the number of output points should not be less than 7. The FX3U type programmable logic controller manufactured by the Mitsubishi Corporation was selected through investigation. The controller has more input and input points to meet the requirements of the end-effector control system.

C. SIMULATION OF THE REFUELING ROBOT GRASPING AND DOCKING

Combined with the above condition setting, the disconnector angle change data are imported into Adams to obtain six Spline curves, q1∼q6, which change with time. The robot was simulated using the cubspl function and the step function in Adams, as shown in Figure 17. This paper has uploaded video of this process; please see the attached video for details. It can be observed from the simulation results that the refueling robot can realize automatic grasping and docking of the quick disconnector.

D. GRABBING AND DOCKING EXPERIMENT OF THE REFUELING ROBOT

Since the communication between the manipulator controller and the upper computer must be conducted through Ethernet, the computer and the network port of the manipulator

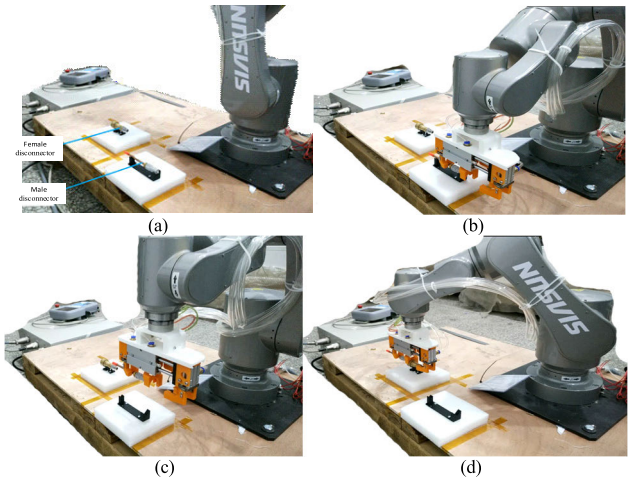

FIGURE 18. (a) Relative position of quick disconnector and the refueling robot. (b)-(d) The process of the refueling robot grasping and docking experiment: (b) P1 position, (c) P2 position, and (d) P3 position.

controller are first connected by the network cable in the experiment, and then remote control of the manipulator can be realized. After successful communication between the upper computer and the refueling robot controller, the upper computer software is used to read the disconnector deflection angle data and transmit it to the refueling robot controller, thereby driving the robot disconnector to move and achieving automatic grasping of the pipeline quick disconnectors.

Initially, the quick disconnectors were placed on two fixed brackets at different positions in the space, as opposed to the refueling robot, as shown in Figure 18(a). By giving instructions to the upper computer, the refueling robot moves to position P1, as shown in Figure 18 (b). The end-effector is continuously controlled to move downward along a straight line until position P2, as shown in Figure 18 (c). The PLC control system drives the end-effector to clamp the positive disconnector. The end-effector is driven by the PLC control system to clamp the male disconnector, and after successful clamping, it returns to P3, as shown in Figure 18 (d). Then, the end-effector holding the male connector reaches position under the control of the driver program, and the female connector is grasped. This paper has an uploaded video of this process; please see the attached video for details.

After the completion of grabbing, the PLC control system controls the on and off electric time of the solenoid valve to achieve the automatic docking of the quick disconnector, as shown in Figure 19. The experiment of the automatic docking process of the quick connector is shown in the figure below.

This paper has uploaded video of this process, please see the attachment video for details. Thus, it can be observed that the automatic grasping and automatic docking of the refueling robot is completed through the experiment by sending instructions from the upper computer.

In order to obtain quantified experimental results of the experimental process, pressure sensor and acceleration sensor are added to measure and acquire experimental data.

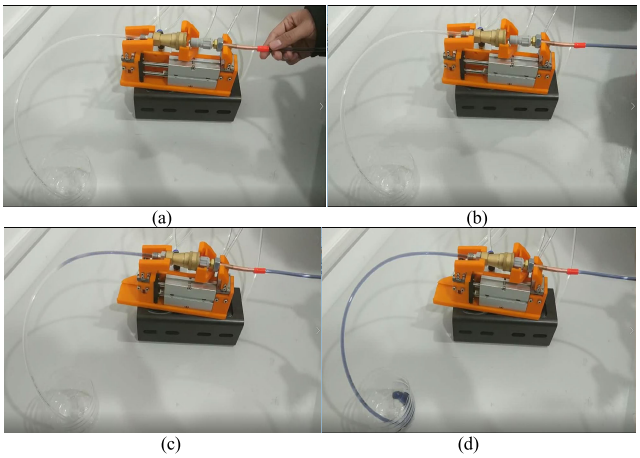

FIGURE 19. Process of the quick disconnector automatic docking.

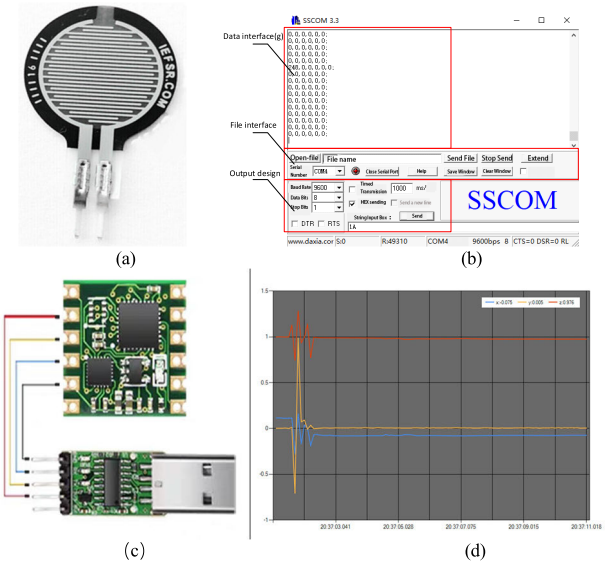

FIGURE 20. (a) RX-D2027 flexible membrane pressure sensor. (b) Operation interface of pressure sensor. (c) Acceleration sensor JY901. (d) Operation interface of acceleration sensor.

The pressure sensor model uses the RX-D2027 flexible membrane pressure sensor, as shown in Figure 20 (a). The RX-D2027 is a flexible standard pressure sensor with an induction diameter of 20 mm and an external force profile of 27 mm. The medium size and thickness and range can be tailored, making this type of sensor available for wide range of applications, such as product evaluation testing, design verification, pressure change detection. The flexible piezoelectric pressure sensor is produced by transferring a nano-sensitive material, a silver paste and the like onto a flexible film substrate through a precision printing process, and drying and solidifying. When the sensor is under pressure, the resistance declines with the increase of pressure. The piezoelectric characteristic is expressed as a power function of the resistance and the pressure. The reciprocal of the resistance is substantially linear with the pressure, the operation interface is as shown in Figure 20 (b).

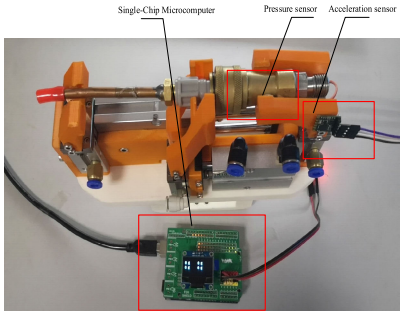

FIGURE 21. Schematic diagram of sensor installation.

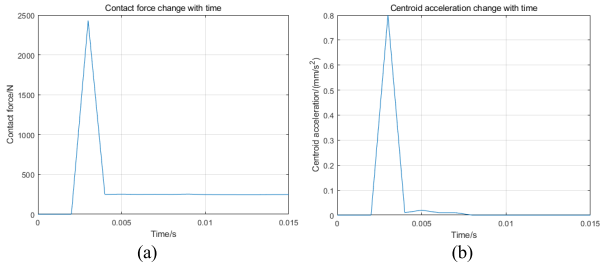

FIGURE 22. (a) Curve of contact force. (b) Curve of centroid acceleration.

TABLE 4. Experimental data (contact force and Centroid acceleration).

Times/s	Contact force/N	Centroid acceleration/ mm/s^2
0.001	0	0
0.002	0	0
0.003	2430.4	0.8
0.004	249.8	0.01
0.005	252.7	0.02
0.006	249.7	0.01
0.007	251.1	0.01
0.008	249.8	0
0.009	253.4	0
0.010	247.2	0
0.011	245.3	0
0.012	244.5	0
0.013	243.8	0
0.014	246.6	0
0.015	247.7	0

The acceleration sensor model is JY901, as shown in Figure 20 (c). The JY901 product is a professional attitude measurement module. It uses MPU9250 chip and joins the core processor. It combines dynamic settlement and dynamic Kalman filter algorithm to ensure that the product accurately output the current module under motion. The motion state data is transmitted through the serial port, and the return rate is 0.1-200HZ. The product supports TTL and LLC communication, which are convenient for users and secondary development, the operation interface is as shown in Figure 20 (d).

The schematic diagram of the installation of the sensor on the end effector is shown in the Figure 21.

The measured data of contact force and centroid acceleration is shown in the Table 4. The curve of contact force and centroid acceleration changing with time can be drawn according to the Table 4, as shown in Figure 22.

The experimental results in this paper well prove the simulation results in the Section 3. According to the experimental data in Table 4 and the change curve of contact force and centroid acceleration with time in Figure 22, the contact force suddenly changes to 2430.4N at the moment of collision and then maintains a stable value of 250 N. This is consistent with the results showed in Figure 12 (a) of Section 3. At the same time, at the moment of conflict, the maximum value of the acceleration along the Y-axis changes to 0.8 , and then stays at 0 in the clamping process, which is consistent with the simulation results in Figure 12 (b). The above experimental results show that in the actual clamping docking process, the variation trend of contact force and acceleration is consistent with the simulation results in Section 3, and finally reaches a stable tendency. Furthermore, advantages of the end effector proposed in this paper are illustrated. The end effector model proposed in this paper has the advantages of closed internal force seal, stable structure and low cost.

V. CONCLUSION

At present, the space station on-orbit service is still developing rapidly, on-orbit refueling operation has not been fully realized. During the process of an on-orbit robotic refueling mission, the pipe disconnectors are artificially docked, and the problems of a low efficiency and a long operation period are common. The docking of the quick disconnector with the gas valve and the liquid valve is realized by manual docking. According to the principle of bionics, a new type of refueling tool is designed, mainly for the automation docking problem of a direct plug-in quick disconnector in the refueling system. Based on the design idea of artificial hand operation, a five-DOF multi-function end-effector with a compact structure and small volume was developed to serve as an automatic butt disconnector of quick pipeline disconnectors. The quick disconnector docking in the refueling system was simplified from the original manual dual-hand operation to a single-end-effector operation with a single manipulator. Compared with a dual-arm robot, a single-arm robot has the advantages of a closed internal force sealing, a stable structure, a higher docking accuracy and a low cost. The research contributions of this paper are as follows:

(1) Mechanism research from the perspective of bionics, the manual docking process of the pipe quick disconnector, the kinematics of the upper limbs and hand of the human body, and the redundant degrees of freedom in the manual docking process are analysed. The quick disconnector docking in the refueling system is simplified from the original

manual dual-hand operation to the single-end-effector operation with a single manipulator.

(2) A five-DOF multi-function end-effector is designed by the design method of the artificial manual operation. Via statics analysis of the fingers of the end-effector, the displacement and stress nephograms of each finger under corresponding constraints and loads are obtained, which can provide a reference for the design optimization of the prototype.

(3) The contact force model of a common rigid body is analysed, and a mathematical model of the contact force between the ''quick disconnector and the robot end-effector'' is established via the equivalent spring damping model method. The expression of the contact force is obtained.

(4) The Adams software package is used to simulate the contact collision process between the effector and the quick disconnector, and the simulation results are analysed to obtain the maximum contact force during the collision process.

(5) A theoretical prototype of the refueling robot end-effector is developed. The air pressure control loop of the end-effector is designed. The experiment is performed by sending instructions from the upper computer, and the automatic grabbing and docking work of the quick disconnectors is completed by the refueling robot.

(6) In order to obtain quantified experimental results of the experimental process, pressure sensor and acceleration sensor are added to measure and acquire experimental data. The experimental results in this paper well prove the simulation results. Furthermore, advantages of the end effector proposed in this paper are illustrated.

The effector cylinders used in the multi-function end-effector designed in this paper are parallel opening and closing types, which have limited opening strokes. The fulcrum opening and closing type effectors can be used in the next-generation prototype. At the same time, the designed end-effector can only be used for automatic docking of the straight in-line pipe disconnectors. It is impossible to use it for screw-type quick butt disconnectors, which are not universal. The paper only studies the contact collision dynamics when the robot end-effector grabs the quick disconnector. In the future, the end-effector can be deeply studied in terms of the speed and force control when grasping the quick disconnector and during the docking process.

REFERENCES

[1] B. Sullivan and D. Akin, ''A survey of serviceable spacecraft failures,'' in *Proc. AIAA Space Conf. Expo.*, vol. 4540, 2001, pp. 1–8.

[2] G. Rekleitis and E. Papadopoulos, ''On-orbit cooperating space robotic servicers handling a passive object,'' *IEEE Trans. Aerosp. Electron. Syst.*, vol. 51, no. 2, pp. 802–814, Apr. 2015.

[3] G. Landis, S. Bailey, and R. Tischler, ''Causes of power-related satellite failures,'' in *Proc. IEEE 4th World Conf. Photovolt. Energy*, vol. 2, May 2006, pp. 1943–1945.

[4] E. Stoll, J. Letschnik, and U. Walter, ''On-orbit servicing,'' *IEEE Robot. Autom. Mag.*, vol. 16, no. 4, pp. 29–33, Dec. 2009.

[5] ''On-orbit satellite servicing study project report,'' NASA, Washington, DC, USA, Tech. Rep., 2010. [Online]. Available: https://sspd.gsfc.nasa.gov/images/NASA_Satellite%20Servicing_Project_Report_0511.pdf

[6] D. E. Hastings, B. L. Putbrese, and P. A. La Tour, ''When will on-orbit servicing be part of the space enterprise?'' *Acta Astronautica*, vol. 127, pp. 655–666, Oct. 2016.

[7] S. Kawase, ''Differential angle tracking for close geostationary satellites,'' *J. Guid., Control, Dyn.*, vol. 16, no. 6, pp. 1055–1060, Nov. 1993.

[8] T. Mulder, ''Orbital express autonomous rendezvous and capture flight operations,'' in *Proc. AAS/AIAA 18th Space Flight Mech. Meeting*, vol. 130, 2008, pp. 1649–1668.

[9] R. Scott and A. Ellery, ''An approach to ground based space surveillance of geostationary on-orbit servicing operations,'' *Acta Astronautica*, vol. 112, pp. 56–68, Jul. 2015.

[10] W.-J. Li, D.-Y. Cheng, X.-G. Liu, Y.-B. Wang, W.-H. Shi, Z.-X. Tang, F. Gao, F.-M. Zeng, H.-Y. Chai, W.-B. Luo, Q. Cong, and Z.-L. Gao, ''On-orbit service (OOS) of spacecraft: A review of engineering developments,'' *Progr. Aerosp. Sci.*, vol. 108, pp. 32–120, Jul. 2019.

[11] A. R. Graham and J. Kingston, ''Assessment of the commercial viability of selected options for on-orbit servicing (OOS),'' *Acta Astronautica*, vol. 117, pp. 38–48, Dec. 2015.

[12] X. Zhang and J. Liu, ''Effective motion planning strategy for space robot capturing targets under consideration of the berth position,'' *Acta Astronautica*, vol. 148, pp. 403–416, Jul. 2018.

[13] I. M. Da Fonseca, L. C. Goes, N. Seito, M. K. Da Silva Duarte, and É. J. De Oliveira, ''Attitude dynamics and control of a spacecraft like a robotic manipulator when implementing on-orbit servicing,'' *Acta Astronautica*, vol. 137, pp. 490–497, Aug. 2017.

[14] W. Yao, X. Chen, Y. Huang, and M. Van Tooren, ''On-orbit servicing system assessment and optimization methods based on lifecycle simulation under mixed aleatory and epistemic uncertainties,'' *Acta Astronautica*, vol. 87, pp. 107–126, Jun. 2013.

[15] H. Benninghoff, F. Rems, and T. Boge, ''Development and hardware-in-the-loop test of a guidance, navigation and control system for on-orbit servicing,'' *Acta Astronautica*, vol. 102, pp. 67–80, Sep. 2014.

[16] J. Li, S. Chen, C. Li, C. Gao, and W. Jing, ''Adaptive control of underactuated flight vehicles with moving mass,'' *Aerosp. Sci. Technol.*, vol. 85, pp. 75–84, Feb. 2019.

[17] J. Li, C. Gao, C. Li, and W. Jing, ''A survey on moving mass control technology,'' *Aerosp. Sci. Technol.*, vols. 82–83, pp. 594–606, Nov. 2018.

[18] J. Li, C. Gao, W. Jing, and Y. Fan, ''Nonlinear vibration analysis of a novel moving mass flight vehicle,'' *Nonlinear Dyn.*, vol. 90, no. 1, pp. 733–748, Oct. 2017.

[19] W. Xu, Z. Mu, T. Liu, and B. Liang, ''A modified modal method for solving the mission-oriented inverse kinematics of hyper-redundant space manipulators for on-orbit servicing,'' *Acta Astronautica*, vol. 139, pp. 54–66, Oct. 2017.

[20] J. H. Saleh, E. S. Lamassoure, D. E. Hastings, and D. J. Newman, ''Flexibility and the value of on-orbit servicing: New customer-centric perspective,'' *J. Spacecraft Rockets*, vol. 40, no. 2, pp. 279–291, Mar. 2003.

[21] W. Xu, B. Liang, B. Li, and Y. Xu, ''A universal on-orbit servicing system used in the geostationary orbit,'' *Adv. Space Res.*, vol. 48, no. 1, pp. 95–119, Jul. 2011.

[22] A. Ellery, J. Kreisel, and B. Sommer, ''The case for robotic on-orbit servicing of spacecraft: Spacecraft reliability is a myth,'' *Acta Astronautica*, vol. 63, nos. 5–6, pp. 632–648, Sep. 2008.

[23] A. M. Long, M. G. Richards, and D. E. Hastings, ''On-orbit servicing: A new value proposition for satellite design and operation,'' *J. Spacecraft Rockets*, vol. 44, no. 4, pp. 964–976, Jul. 2007.

[24] G. Hirzinger, K. Landzettel, B. Brunner, M. Fischer, C. Preusche, D. Reintsema, A. Albu-Schäffer, G. Schreiber, and B.-M. Steinmetz, ''DLR's robotics technologies for on-orbit servicing,'' *Adv. Robot.*, vol. 18, no. 2, pp. 139–174, Jan. 2004.

[25] E. Stoll, U. Walter, J. Artigas, C. Preusche, P. Kremer, G. Hirzinger, J. Letschnik, and H. Pongrac, ''Ground verification of the feasibility of telepresent on-orbit servicing,'' *J. Field Robot.*, vol. 26, no. 3, pp. 287–307, Mar. 2009.

[26] A. Flores-Abad, O. Ma, K. Pham, and S. Ulrich, ''A review of space robotics technologies for on-orbit servicing,'' *Progr. Aerosp. Sci.*, vol. 68, pp. 1–26, Jul. 2014.

[27] D. M. Waltz and F. Cepollina, *On-Orbit Servicing of Space Systems*. Malabar, FL, USA: Krieger Publishing Company, 1993.

[28] Z. Cheng, X. Hou, X. Zhang, L. Zhou, J. Guo, and C. Song, "In-orbit assembly mission for the space solar power station," *Acta Astronautica*, vol. 129, pp. 299–308, Dec. 2016.
[29] G. Leisman, A. Wallen, S. Kramer, and W. Murdock, "Analysis and preliminary design of on-orbit servicing architectures for the GPS constellation," in *Proc. AIAA Space Technol. Conf. Expo.*, 1999, p. 4425.
[30] J. H. Saleh, E. Lamassoure, and D. E. Hastings, "Space systems flexibility provided by on-orbit servicing: Part 1," *J. Spacecraft Rockets*, vol. 39, no. 4, pp. 551–560, Jul. 2002.
[31] E. Lamassoure, J. H. Saleh, and D. E. Hastings, "Space systems flexibility provided by on-orbit servicing: Part 2," *J. Spacecraft Rockets*, vol. 39, no. 4, pp. 561–570, Jul. 2002.
[32] R. Miller, M. Minsky, and D. Smith, "Space applications of automation, robotics and machine intelligence systems (ARAMIS)," NASA, Washington, DC, USA, Tech. Rep. NASA-CR-3735, NAS 1.26:3735, SSL-31-83, 1982, vol. 2.
[33] S. Dubowsky, "Advanced methods for the dynamic control of high performance robotic devices and manipulators with potential for applications in space," NASA, Washington, DC, USA, Tech. Rep. CR-181061, 1987.
[34] N. Davinic, S. Chappie, A. Arkus, and J. Greenberg, "Spacecraft modular architecture design study-cost benefit analysis of on-orbit satellite servicing," in *Proc. 48th Int. Astron. Congr. (IAF)*, Turin, Italy, 1997. [Online]. Available: https://scholar.google.com.hk/scholar?cluster=18459666763933242 42&hl=zh-CN&as_sdt=2005&sciodt=0,5
[35] *NASA Technology Roadmap TA 4: Robotics and Autonomous Systems*, NASA, Washington, DC, USA, 2015.
[36] A. Medina, A. Tomassini, M. Suatoni, M. Avilés, N. Solway, I. Coxhill, I. S. Paraskevas, G. Rekleitis, E. Papadopoulos, R. Krenn, A. Brito, B. Sabbatinelli, B. Wollenhaupt, C. Vidal, S. Aziz, and G. Visentin, "Towards a standardized grasping and refuelling on-orbit servicing for geo spacecraft," *Acta Astronautica*, vol. 134, pp. 1–10, May 2017.
[37] M. Machado, P. Moreira, P. Flores, and H. M. Lankarani, "Compliant contact force models in multibody dynamics: Evolution of the Hertz contact theory," *Mechanism Mach. Theory*, vol. 53, pp. 99–121, Jul. 2012.
[38] L.-B. Wee and M. Walker, "On the dynamics of contact between space robots and configuration control for impact minimization," *IEEE Trans. Robot. Autom.*, vol. 9, no. 5, pp. 581–591, Oct. 1993.
[39] O. Ma, K. Buhariwala, N. Roger, J. Maclean, and R. Carr, "MDSF—A generic development and simulation facility for flexible, complex robotic systems," *Robotica*, vol. 15, no. 1, pp. 49–62, Jan. 1997.
[40] O. Ma and J. Wang, "Model order reduction for impact-contact dynamics simulations of flexible manipulators," *Robotica*, vol. 25, no. 4, pp. 397–407, Jul. 2007.
[41] M. Shibli, F. Aghili, and C.-Y. Su, "Modeling of a free-flying space robot manipulator in contact with a target satellite," in *Proc. IEEE Conf. Control Appl.*, Aug. 2005, pp. 559–564.
[42] D. Nenchev and K. Yoshida, "Impact analysis and post-impact motion control issues of a free-floating Space robot subject to a force impulse," *IEEE Trans. Robot. Autom.*, vol. 15, no. 3, pp. 548–557, Jun. 1999.
[43] O. Ma, A. Flores-Abad, and T. Boge, "Use of industrial robots for hardware-in-the-loop simulation of satellite rendezvous and docking," *Acta Astronautica*, vol. 81, no. 1, pp. 335–347, Dec. 2012.
[44] S. Abiko, N. Uyama, T. Ikuta, K. Nagaoka, K. Yoshida, J. Nakanishi, and M. Oda, "Contact dynamic simulation for capture operation by snare wire type of end effector," in *Proc. Int. Symp. Artif. Intell., Robot. Automat. Space*, 2012. [Online]. Available: https://scholar.google.com.hk/scholar?hl=zh-CN&as_sdt=0%2C5&q=%E2%80%98Contact+dynamic+simulation+for+capture+operation+by+snare+wire+type+of+end+effect&btnG=
[45] N. Uyama, K. Nagaoka, and K. Yoshida, "Experimental evaluation of contact-impact dynamics between a space robot with a compliant wrist and a free-flying object," in *Proc. Int. Symp. Artif. Intell., Robot. Automat. Space*, 2012, pp. 1–7.
[46] H. Sawada, S. Szuki, and M. Oda, "A contact dynamics analysis of spacecraft capturing and rigidizing," in *Proc. 17th Workshop JAXA Astrodyn. Flight Mech.*, 2007, pp. 1–6.
[47] G. Gilardi and I. Sharf, "Literature survey of contact dynamics modelling," *Mechanism Mach. Theory*, vol. 37, no. 10, pp. 1213–1239, Oct. 2002.

JINGUO LIU (Senior Member, IEEE) received the Ph.D. degree in mechatronics from the Shenyang Institute of Automation (SIA), Chinese Academy of Sciences (CAS), in 2007.

Since January 2011, he has been a Full Professor with SIA, CAS. He has also been the Assistant Director of the State Key Laboratory of Robotics, since 2008, and has been the Associate Director of the Center for Space Automation Technologies and Systems, since 2015. His research interests include bio-inspired robotics and space robot. He has authored/coauthored three books, over 100 articles and holds 50 patents in above areas. He is a Senior Member of the IEEE Technical Committee on Safety, Security, and Rescue Robotics, the IEEE Technical Committee on Marine Robotics, and the Chinese Mechanical Engineering Society. He received the T. J. TARN Best Paper Award in Robotics from the 2005 IEEE International Conference on Robotics and Biomimetics, the Best Paper Award of the Chinese Mechanical Engineering Society, in 2007, the Best Paper Nomination Award from 2008 International Symposium on Intelligent Unmanned Systems, the Best Paper Award from 2016 China Manned Space Academic Conference, and the Outstanding Paper Award from 2017 International Conference on Intelligent Robotics and Applications, and the Best Paper Award from 2018 International Conference on Electrical Machines and systems. He serves as an Associate Editor of several journals, such as *Mechanical Sciences*, *Advances in Mechanical Engineering*, and *Chinese Journal of Mechanical Engineering*.

YUCHUANG TONG received the bachelor's degree in process equipment and control engineering from the Beijing University of Chemical Technology, in 2017. She is currently pursuing the Ph.D. degree in mechatronic engineering from the Shenyang Institute of Automation (SIA), Chinese Academy of Sciences (CAS). Her research interests mainly include end-effector, bio-inspired robot, and space robot.

YUNJUN LIU received the B.S. degree from the China University of Geosciences, Wuhan, in 2016, and the M.S. degree from the Shenyang Institute of Automation (SIA), in 2019. His main research interests include robotics, end-effector, and space robot.

YUWANG LIU (Member, IEEE) received the Ph.D. degree in robotics from the Shenyang Institute of Automation, Chinese Academy of Sciences, in 2010.

Since then, he has been working with the Shenyang Institute of Automation, Chinese Academy of Sciences. As a Project Leader or Core-Backbone, he involved in National Natural Science Foundation of China (NSFC), National High-Tech Research and Development Program of China (863 Program), National Science and Technology Major Project of CNC, and Key Program of the Chinese Academy of Sciences. He is currently working on robotic mechanism for the application of special environmental science, under-actuated and kinematic coupling mechanism, dexterous operations of robots and multifingered crawling theory, mechatronics design, and precision-driven sensor systems.